Enhancing Active Power Regulation of VSM through Impedance Estimation-Aided Feedforward Control

Jae-Young Park, Jin Soo Lee, Ki-Hyun Kim, Jae Hyung Roh, and Jong-Bae Park
Department of Electrical and Electronics Engineering
Konkuk University
Seoul, Republic of Korea
jypark10@konkuk.ac.kr

***Abstract*—This paper presents a novel feedforward control strategy for the virtual synchronous machine (VSM) to enhance active power regulation. The proposed method directly adjusts the phase angle reference of the VSM in response to the active power reference signal, enabling rapid, accurate active power control. Additionally, an impedance estimation scheme for the grid line is developed to facilitate practical implementation of the proposed strategy. The effectiveness of the proposed methods is thoroughly verified through simulations in a controller hardware-in-the-loop framework.**

***Index Terms*—Grid forming, virtual synchronous machine, feedforward control, active power regulation, grid parameter impedance estimation, control hardware-in-the-loop simulation.**

INTRODUCTION

Grid-forming (GFM) inverters play a key role in achieving carbon-neutral grids by enabling renewable energy integration while maintaining grid stability. Among various GFM strategies, the virtual synchronous machine (VSM) is one of the most widely adopted industrial solutions [1]. In the VSM, the inverter phase angle is determined by emulating the swing equation, resulting in a second-order active power response governed by the virtual inertia and frequency damping parameters. Improper tuning of these parameters can lead to sluggish or oscillatory active power dynamics [2]. In modern low-inertia power systems, however, fast and accurate active power control is increasingly critical for mitigating system frequency deviations. Although the active power response can be adjusted by tuning the virtual inertia and damping values, this approach is fundamentally limited by an inherent trade-off: improved active power tracking comes at the expense of weakened inertial and damping support to the grid.

To address this limitation, various enhancements to the VSM have been proposed. Acceleration control schemes using optimal or adaptive gain design have been investigated to improve the active power response while maintaining stability [3], [4], but they often require complex gain tuning, which limits their practical applicability. More recently, feedforward control (FC) strategies have been explored, in which frequency-related [5] or phase-related [6] signals are fed forward to accelerate the active power response. However, the active power dynamics in these methods remain coupled with the inertia and damping parameters, leaving the fundamental trade-off unresolved. Moreover, most existing FC-based methods require grid impedance information for parameter design; however, this information is often unavailable to a unit inverter in practice. Although impedance estimation techniques based on harmonic injection or step power changes have been reported [7], [8], these approaches may interfere with normal operation and typically assume constant grid voltage, which does not hold under real-world conditions.

This paper proposes a novel GFM strategy that integrates a grid-aware FC path into the VSM method. The proposed method allows the reference signal to directly adjust the phase angle, bypassing the slow swing-equation dynamics to achieve precise active power control while preserving inertial and damping characteristics. A grid impedance estimation method that uses only locally available measurements is also developed for autonomous implementation. The effectiveness of the proposed method is validated via controller hardware-in-the-loop (HIL) simulations. The proposed strategy is well suited to inverter-dominated grids requiring fast, accurate active power regulation under low-inertia conditions.

DEVELOPMENT OF THE PROPOSED METHODS

A. The FC-intergrated VSM Control Strategy

The schematics of a grid-connected GFM inverter under study and the proposed control method, FC-integrated VSM (FC-VSM), are shown in Fig. 1. As depicted in Fig. 1(b), the FC-VSM incorporates FC path with the traditional VSM, enabling the active power reference P_{ref} to bypass the slow dynamics of the swing equation and adjust the phase angle reference θ_e immediately. This advancement significantly improves the regulation of the active power P to P_{ref}. To clarify the advantage of incorporating the FC path into the VSM strategy, we compare the P responses of the traditional VSM and FC-VSM. First, disregarding the FC path in Fig. 1(b) results in the P response of the traditional VSM, as:

This work was supported by the Korea Institue of Energy Technology Evaluation and Planning(KETEP) and the Ministry of Climate, Energy & Environment(MCEE) of the Republic of Korea (RS-2025-02422969).

979-8-3315-8138-1

(a)

(b)

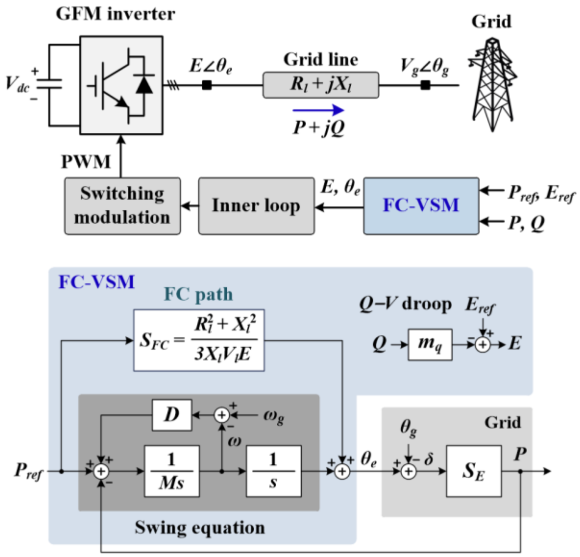

Fig. 1. Schematic diagrams of (a) a GFM inverter under study and (b) the proposed FC-VSM control strategy.

$$P = \frac{1}{S_E^{-1}Ms^2 + S_E^{-1}Ds + 1} P_{ref} - \frac{Ms}{S_E^{-1}Ms^2 + S_E^{-1}Ds + 1}\omega_g \quad (1)$$
$$= G_r(s)\cdot P_{ref} - G_\omega(s)\cdot\omega_g .$$

where ω_g is the grid frequency; M and D denote the virtual inertia and damping; and S_E is the synchronizing power coefficient derived from the steady-state expression of P in (2) with respect to the power angle $\delta = \theta_e - \theta$ as follows:

$$P = 3\frac{R_l E(E - V_g\cos\delta) + X_l V_g E\sin\delta}{R_l^2 + X_l^2} \cong 3\frac{X_l V_g E}{R_l^2 + X_l^2}\delta , \quad (2)$$

$$\text{and } S_E = \frac{\partial P}{\partial \delta} = 3\frac{R_l V_g E\sin\delta + X_l V_g E\cos\delta}{R_l^2 + X_l^2} \cong \frac{3X_l V_g E}{R_l^2 + X_l^2} , \quad (3)$$

where V_g and θ_g are the magnitude and phase angle of the grid voltage; R_l and X_l are the grid resistance and reactance; E is the terminal voltage magnitude of the GFM inverter. The approximations in (2) and (3) assume nominal voltages and small power-angle deviations under normal operating conditions [6].

As shown in (1), the P response is characterized by two transfer functions: $G_r(s)$ and $G_\omega(s)$. They represent the grid-supporting performance of the traditional VSM [1]. In fact, $G_r(s)$ represents the reference tracking behavior, which is crucial for real-time load following for grid frequency regulation. $G_\omega(s)$ defines the inertial and damping responses to suppress instantaneous changes in grid frequency ω_g. As shown in (1), $G_r(s)$ and $G_\omega(s)$ are governed commonly by M and D. Thus, it is important to properly tune them to achieve the superior grid-supporting performance. However, adjusting M and D results in a trade-off between reference tracking behavior and inertial and damping responses: e.g., reducing M and D allows for P to better track P_{ref} but weakens the inertia and damping support for the grid [3].

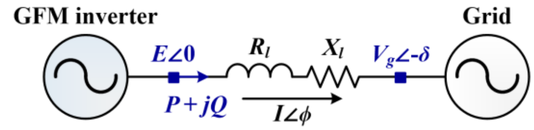

Fig. 2. Equivalent circuit representation of the system shown in Fig.1(a).

In contrast, from Fig. 1(b), the P response of the FC-VSM is derived, as:

$$P = \frac{S_{FC}Ms^2 + S_{FC}Ds + 1}{S_E^{-1}Ms^2 + S_E^{-1}Ds + 1} P_{ref} - \frac{Ms}{S_E^{-1}Ms^2 + S_E^{-1}Ds + 1}\omega_g \quad (4)$$
$$= H_r(s)\cdot P_{ref} - H_\omega(s)\cdot\omega_g .$$

where S_{FC} is the FC gain. Similar to the traditional VSM, $H_r(s)$ defines the reference tracking behavior and $H_\omega(s)$ determines the inertial and damping responses of the FC-VSM. Notably, (4) indicates that setting S_{FC} to S_E^{-1} yields a unity gain for $H_r(s)$, resulting the following P response:

$$P = P_{ref} - H_\omega(s)\omega_g , \quad (5)$$

As shown in (5), P tracks P_{ref} in real time. Furthermore, $H_\omega(s)$ in (4) remains consistent with $G_\omega(s)$ in (2), implying that the FC path enhances reference tracking behavior without compromising inertia and damping responses.

B. Grid-Side Parameter Estimation Method

However, as indicated in (3), setting S_{FC} = S_E^{-1} requires knowledge of grid-side parameters, i.e., R_l, X_l, and V_g, which are typically unavailable to a unit inverter. To enable autonomous implementation of the proposed FC-VSM strategy, a grid-side parameter estimation method based solely on locally available measurements is developed. Fig. 2 presents an equivalent circuit representation of the system shown in Fig. 1(a). In this representation, R_l, X_l, and V_g can be estimated by minimizing the sum of the residuals as follows:

$$(R_l, X_l, V_g) \cong \underset{\hat{R}_l,\, \hat{X}_l,\, \hat{V}_g}{\arg\min}\, r_P + r_Q + r_E , \quad (6)$$

$$\text{where } r_P = \sum_{k=1}^{N_d}\left| P_k - \hat{V}_g I_k\cos(\delta_k + \phi_k) - I_k^2\hat{R}_l \right| , \quad (7)$$

$$r_Q = \sum_{k=1}^{N_d}\left| Q_k + \hat{V}_g I_k\sin(\delta_k + \phi_k) - I_k^2\hat{X}_l \right| , \quad (8)$$

$$r_E = \sum_{k=1}^{N_d}\left| E_k - \sqrt{\left(\hat{V}_g\cos\delta_k + A_k\right)^2 + \left(\hat{V}_g\sin\delta_k + B_k\right)^2} \right| , \quad (9)$$

$$A_k = I_k\hat{R}_l\cos\phi_k - I_k\hat{X}_l\sin\phi_k , \quad (10)$$

$$\text{and } B_k = I_k\hat{X}_l\cos\phi_k + I_k\hat{R}_l\sin\phi_k . \quad (11)$$

In (6)–(11), $\hat{\bullet}$ denotes the estimated value of •; the subscript k indicates the k-th sample among N_d data points; and I_k and ϕ_k

979-8-3315-8138-1

Algorithm I: GSA for Grid-Side Information Estimation

Input: $\mathbf{P_D}$, $\mathbf{Q_D}$, $\mathbf{E_D}$, $\mathbf{X_{min}}$, $\mathbf{X_{max}}$, and N_s
// Initialization
Set $[\hat{R}_l, \hat{X}_l, \hat{V}_g] = \mathbf{X_{min}}$
Compute $r_{cand} = r_P + r_Q + r_E$ using (7)–(9)
Set $[R_l, X_l, V_g] = [\hat{R}_l, \hat{X}_l, \hat{V}_g]$ and $r_{opt} = r_{cand}$
// Updating estimates and residual
Compute $\mathbf{D} = [D_r, D_x, D_v] = (\mathbf{X_{max}} - \mathbf{X_{min}})/N_s$
For l from 1 to N_s **do**
Compute $\hat{R}_l = R_{l\_min} + l \cdot D_r$
  For m from 1 to N_s **do**
  Compute $\hat{X}_l = X_{l\_min} + m \cdot D_x$
    For n from 1 to N_s **do**
    Compute $\hat{V}_g = V_{g\_min} + n \cdot D_v$
    Compute $r_{cand} = r_P + r_Q + r_E$ using (7)–(9)
      If $r_{cand} < r_{opt}$ **then**
        Set $[R_l, X_l, V_g] = [\hat{R}_l, \hat{X}_l, \hat{V}_g]$ and $r_{opt} = r_{cand}$
Return R_l, X_l, V_g

are the magnitude and phase angle of the injected current by the GFM inverter, computed using $I_k \cdot (\cos\phi_k + j\sin\phi_k) = (P_k - jQ_k)/E_k$. Specifically, (7) and (8) correspond to active and reactive power conservation in Fig. 2, while (9) relates E and V_g considering impedance-induced voltage drops.

A challenge arises, however, because δ_k in (8) and (9) is not directly measurable at the terminal of the GFM inverter, as it involves the grid angle θ_{g_k}: $\delta_k = \theta_{e,k} - \theta_{g,k}$. To resolve this, we evaluate δ_k using (2) with locally available data, as:

$$\delta_k \cong \frac{\hat{R}_l^2 + \hat{X}_l^2}{\hat{X}_l \hat{V}_l E_k} P_k . \tag{12}$$

By substituting (12) into (7)–(9), the estimation problem (6)–(11) is simplified only to require data on P_k, Q_k, and E_k, all of which are readily measurable at a GFM inverter terminal.

The optimal solution of (6) can be easily obtained using a grid search algorithm (GSA) [9]. Algorithm I shows a pseudocode of the GSA for solving the proposed estimation problem. $\mathbf{P_D}$, $\mathbf{Q_D}$, and $\mathbf{E_D}$ are sampled data vectors of P_k, Q_k, and E_k, respectively. N_s is the number of searching segments. $\mathbf{X_{min}}$ and $\mathbf{X_{max}}$ are the minimum and maximum estimates of R_l, X_l, and V_g: $\mathbf{X_{max}} = [\overline{R}_l, \overline{X}_l, \overline{V}_g]$ and $\mathbf{X_{min}} = [\underline{R}_l, \underline{X}_l, \underline{V}_g]$. In distribution networks, R_l and X_l typically range from 0.01 to 1.0 pu, depending on line length and configuration, while V_g is generally maintained between 0.90 and 1.1 pu to meet voltage regulation standards.

VERIFICATION OF THE PROPOSED METHODS

Fig. 3 shows the C-HIL testing setup used to validate the proposed methods. The setup mainly consists of a Typhoon HIL Real-Time simulator, controller board, and measurement equipment. The dynamic models of the three-phase (3-ph) ac grid, line impedances, and GFM inverter unit are established and emulated in real-time in The Typhoon HIL simulator. The voltages, currents, and real/reactive power from the model are continuously monitored using an oscilloscope. Table I lists the model parameters. In addition, all control algorithms are implemented on the controller board, which is based on a TI TMS320F28377 DSP. A DC power supply provides operating power for the controller board.

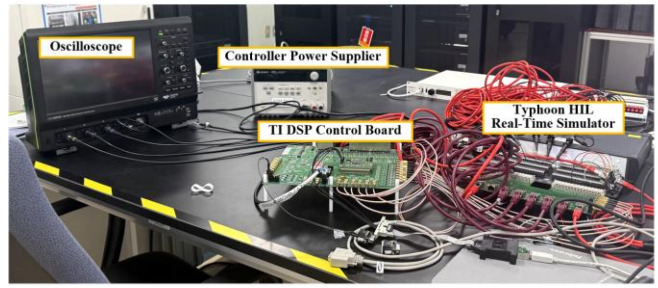

Fig. 3. A controller HIL testing setup developed for the verification of the proposed methods

TABLE I
PARAMETERS OF THE CONTROLLER-HIL TESTING MODEL

Model	Description	Parameter	Value
Grid	Voltage and frequency	V_g, f_g	220 V_{rms}, 60 Hz
	Line parameters	R_l, L_l	0.30 Ω, 6.65 mH
GFM inverter	Switching frequency	f_{sw}	20 kHz
	Rated power	S_{rated}	25 kVA
	Nominal ac/dc voltages	E, V_{dc}	220 V_{rms}, 750 V_{dc}
	LCL filter	L_{fi}, L_{fg}, C_f	4.4, 2.2 mH, 1 μF
	Inertia and damping	M, D	18 s, 214.7 pu
	Q–V droop control gain	m_q	0.015 pu

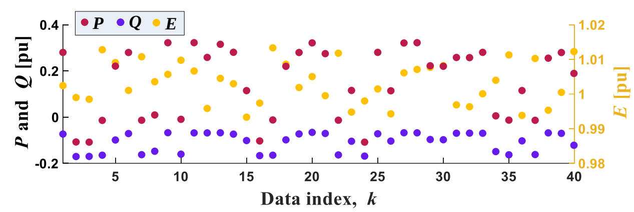

Fig. 4. The P, Q, and E data sampled for the grid estimation.

TABLE II
ESTIMATION RESULTS FOR THE GRID-SIDE PARAMETERS

Variable	Actual value	Estimated value	Accuracy
R_l	0.30 Ω	0.286 Ω	95.3 %
X_l	2.51 Ω	2.466 Ω	98.2 %
V_g	225.5 V	225.28 V	99.9 %
S_{FC}	0.086 pu	0.0845 pu	98.3 %

C. *Verification of Grid-Side Information Estimation Method*

The estimation method for grid impedance and voltage, introduced in Section II-B, was first evaluated. In this test, V_g was set to 1.025 pu, and the GFM inverter initially operated under the traditional VSM with $S_{FC} = 0$. For data collection, P, Q, and E were measured while varying P_{ref} and E_{ref}. Fig. 4 shows the 40 sampled data points of P, Q, and E. Using these data as inputs to the estimation models in (6)–(9), R_l, X_l, and V_g were estimated, as summarized in Table II. The proposed method achieved estimation errors below 5%, with a total

979-8-3315-8138-1

computation time of 3 min 48 s, which is sufficiently fast for quasi-static grid parameter identification and periodic gain updates. This accurate estimation enables precise evaluation of SFC and facilitates decentralized and autonomous implementation of the proposed FC-VSM control strategy.

D. Comparative Verification of FC-VSM Control Strategy

We validated the FC-VSM strategy by comparing its response with that of the traditional VSM. Fig. 5 shows the P responses of the FC-VSM and traditional VSM to stepwise variations in P_{ref}. The P of the traditional VSM slowly followed P_{ref}, due to the second-order dynamics discussed in (2). In contrast, the FC-VSM enabled P to readily reach P_{ref}, which is consistent with the analysis in (5). Fig. 6 presents the 3-ph currents and voltages of the FC-VSM near $t = t_m$, particularly when the active power increased the most. Through the direct correction of the phase angle in response to the active power reference, the FC allowed for rapid changes in the currents while stably maintaining the voltages, thereby enabling quick adjustments of the active power.

We also compared the P responses of the FC-VSM and the traditional VSM to the change of ω_g presented in Fig. 7(a). As shown in Fig. 7(b), both P responses are consistent, confirming that the FC-VSM achieves improved active power reference tracking while ensuring the same level of inertial and damping responses as the traditional VSM.

E. Impact of Parameter Estimation Errors

Additional simulations were conducted to evaluate the impact of parameter estimation errors. Specifically, to emulate a weaker grid condition, R_l and L_l were increased by 10% from their nominal values in Table I, resulting in an S_{FC} estimation error of 11.9%. As shown in Fig. 8, the presence of estimation errors introduces an overshoot in the P response, but the proposed FC-VSM consistently exhibits improved dynamic performance compared to the conventional VSM. These results demonstrate that the proposed method maintains robust active power regulation capability even in the presence of moderate parameter estimation uncertainties.

CONCLUSION

This study proposed an FC-VSM strategy to enhance the active power response of VSM-controlled GFM inverters. By integrating a feedforward path with decentralized impedance estimation, the proposed method enables fast and autonomous active power regulation while preserving inertia and damping characteristics. The effectiveness and robustness of the approach was validated through controller HIL simulations. The FC-VSM strategy is suitable for inverter-dominated, low-inertia power systems. Future work will extend the validation to power HIL experiments, including fault and voltage sag conditions, as well as multi-inverter operation.

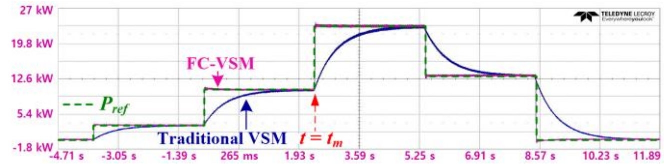

Fig. 5. The P responses of the FC-VSM and the traditional VSM to P_{ref} variations.

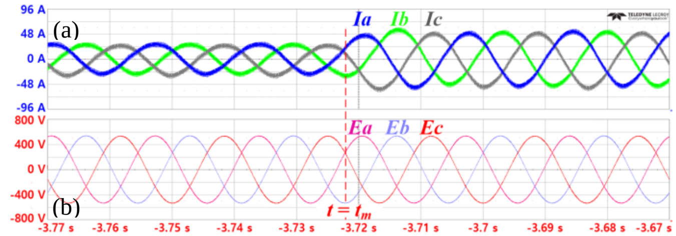

Fig. 6. (a) The currents and (b) the line-to-line voltages of the FC-VSM near $t = t_m$.

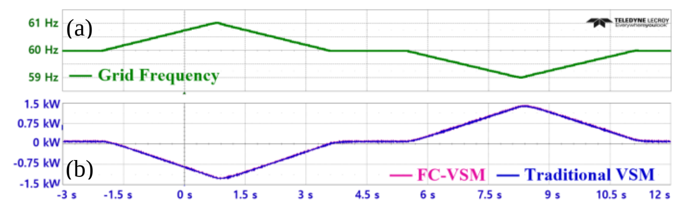

Fig. 7. (a) The change of grid frequency and (b) the corresponding P responses of the FC-VSM and the traditional VSM.

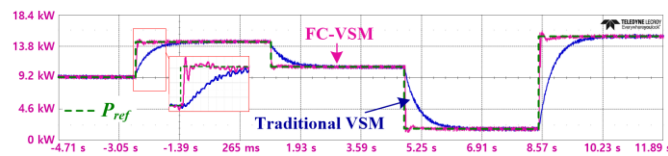

Fig. 8. Comparison of P responses under the parameter error.

REFERENCE

[1] Grid Code Committee, *Grid Code GC0137: Minimum Specification Required for Provision of GB Grid Forming Capability*, NGESO. 2022.

[2] W. Zhang *et al*., "Synchronous Power Controller With Flexible Droop Characteristics for Renewable Power Generation Systems," *IEEE Trans. Sustain. Energy*, vol. 7, no. 4, pp. 1572–1582, Oct. 2016.

[3] B. Pournazarian *et al*., "Simultaneous Optimization of Virtual Synchronous Generators Parameters and Virtual Impedances in Islanded Microgrids", *IEEE Trans. Smart Grid*, vol. 13, no. 6, pp. 4202–4217, Nov. 2022.

[4] F. Wang *et al*., "An Adaptive Control Strategy for Virtual Synchronous Generator", *IEEE Trans. Ind. Appl.*, vol. 54, no. 5, pp. 5124–5133, Oct. 2018.

[5] M. Chen *et al*., "Active Power Oscillation Damping Based on Acceleration Control In Paralleled Virtual Synchronous Generators System", *IEEE Trans. Power Electron.*, vol. 36, no. 8, pp. 9501–9510, Aug. 2021.

[6] M. Li *et al*., "Phase Feedforward Damping Control Method for Virtual Synchronous Generators", *IEEE Trans. Power Electron.*, vol. 37, no. 8, pp. 9790–9806, Aug. 2022.

[7] D. K. Alves *et al*., "Real-Time Wavelet-Based Grid Impedance Estimation Method," *IEEE Trans. Ind. Electron*., vol. 66, no. 10, pp. 8263–8265, Oct. 2019.

[8] N. Mohammed, T. Kerekes, and M. Ciobotaru, "An Online Event-Based Grid Impedance Estimation Technique Using Grid-Connected Inverters," *IEEE Trans. Power Electron*., vol. 36, no. 5, pp. 6106–6117, May 2021.

[9] H. D. Vinod and C. R. Rao, Handbook of Statistics, Ed. Amsterdam, Netherlands: Elsevier, 2019.

979-8-3315-8138-1